Research Article | Vol. 10, No. 2 | 1 Feb 2019 | BIOMEDICAL OPTICS EXPRESS 868
Biomedical Optics EXPRESS

Monte Carlo simulation of light scattering in tissue for the design of skin-like optical devices

HAICHENG LI,[1,2] CHANGXING ZHANG,[1,2] AND XUE FENG[1,2,*]

[1]AML, Department of Engineering Mechanics, Tsinghua University, Beijing, 100084, China
[2]Center for Flexible Electronics Technology, Tsinghua University, Beijing, 100084, China
*fengxue@tsinghua.edu.cn

Abstract: Measurement techniques based on optics, with the characteristics of noninvasive or non-destructive detection and high accuracy, offer excellent properties for application in various scenarios. Skin-like optical devices capable of deforming with human skin play major roles in future biomedical applications such as clinical diagnostics or biological healthcare. Unlike traditional rigid devices, the skin-like optical device is conformal to the skin because of the flexibility and stretchability. However, the detected signals based on light intensity are very sensitive to the light path. As a result, the accuracy and efficiency of the skin-like device will be influenced owing to deformation. In this work, for optimizing the design of the skin-like optical device, we use the Monte Carlo method to investigate the light distribution after scattered and absorbed by a human tissue. Different parameters of light source and blood vessels are used to simulate the device and human tissue deformation respectively. The characteristics of the exited light are then summarized and analyzed to study the influence of the deformation. The simulation shows that the deformation of the device and human tissue will produce non-linear effects on the characteristics of the exited lights. Finally, we design and fabricate a skin-like device using the simulation results and use it to monitor photoplethysmogram signals. This work will aid in the design of skin-like optical devices in the future.

1. Introduction

Measurement techniques [1–3] based on optics offer noninvasive detecting ability in different fields such as mechanical properties monitoring [4], medical healthcare [5,6] and surface topography [7,8]. Optical devices, composed of light-emitting and receiving elements, are widely applied to in-vitro human vital signs monitoring [9,10] and medical imaging system [11]. The physiological information measured by these optical devices play a key role in health assessment for daily life and clinical treatments. The optical device could allow for non-contact or noninvasive vital signs monitoring, which is highly desirable for using in clinical diagnosis and daily healthcare [12–14]. For example, the blood oxygen saturation can be measured by detecting the absorption of light by blood vessels and other tissue [15]. The principles of these optical devices depend on Beer-Lambert Law and spectral analysis. These devices are very sensitive and accurate owing to the application of optical monitoring.

Skin-like devices [16–20] have received increasing attention in the last couple of decades because of the potential applications in healthcare [21–23] and clinical treatment [24]. Unlike traditional devices, skin-like devices have the capability of deformation while being mounted on the skin [25,26]. However, the accuracy of these devices is affected when the deformation changes the optical path. These distortions cannot be offset by precise back-end circuit because of the randomness and no-regularity. Furthermore, the deformation of the skin itself is also an important interference to vital signs monitoring. When the skin is squeezed or stretched, the tissues and blood vessels are forced to redistribute. Thus, the light scattering

#345145 https://doi.org/10.1364/BOE.10.000868
Journal © 2019 Received 5 Sep 2018; revised 31 Oct 2018; accepted 22 Nov 2018; published 24 Jan 2019

Biomedical Optics EXPRESS

and absorption by human tissues are changed. Therefore, the light path influenced by skin and tissue deformation needs to be evaluated when designing a skin-like optical device. In recent work, some theoretical research has been done on the light migration or scattering profile in human tissues [27–29]; however, no research focused on the influence of device and tissue deformation to detected signals. In conclusion, theoretical research of the relationship between light signals and device or skin deformations is highly desirable.

For optimizing the designs of the skin-like optical device for human vital signs monitoring, we use the Monte Carlo (MC) simulation to investigate the distribution of exited light from the human tissue, including reflected and transmitted light. We change the characteristics of the incident light for simulating the device deformation, including incident angle, intensity and light source size. Then we set the different parameters of blood vessel for simulating the skin deformation, including vessel diameter, density and range. The optical path of the light propagation in tissue is calculated for different parameters of vessel or light source, and the distribution of the exited light is analyzed to optimize the design of the skin-like device. Finally, we design and fabricate a skin-like optical device, and use it to monitor photoplethysmogram (PPG) signal. The research opens up new prospects for the design of optical devices, especially for skin-like or flexible optical devices.

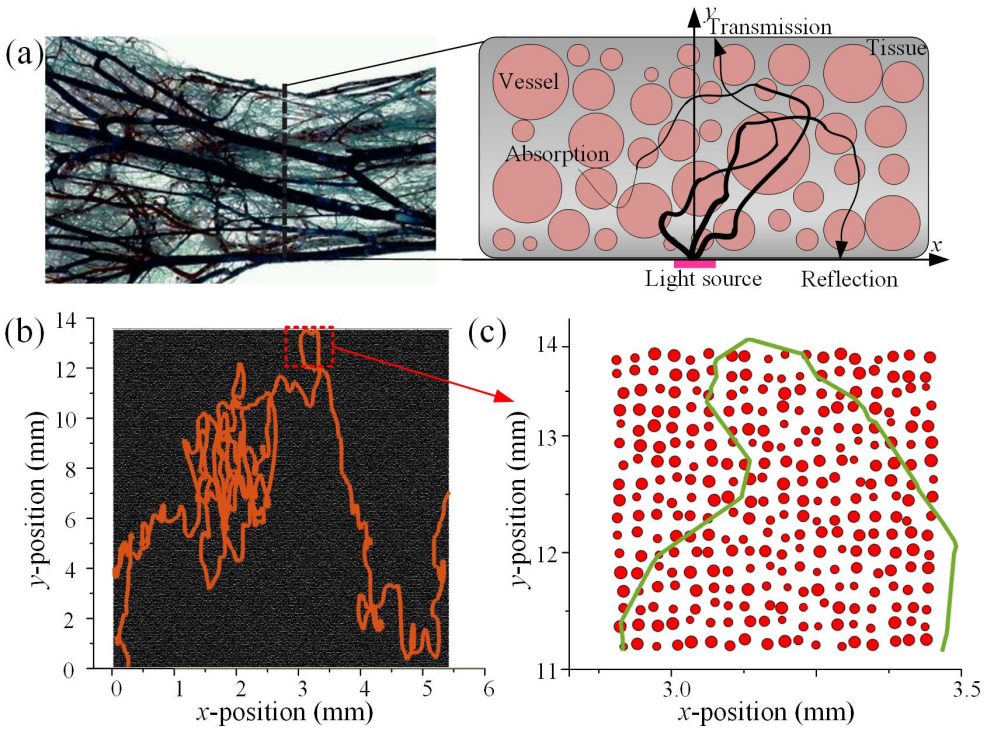

Fig. 1. Schematic diagram of the simulated two-dimensional (2D) model and the light path in the model. (a) Left: The vascular casting of human wrist. Right: the simulated 2D model of the cross-sectional view of wrist [30]. Blood vessels (red circles) with different sizes are randomly placed in a rectangular tissue (black area), while the light source is placed at the middle position of bottom. (b) One simulated light path in the model. (c) Zoom-in image of the rectangle area in the blood vessels, where red circles represent blood vessels.

2. Model of the human blood vessels

A two-dimensional (2D) model of human subcutaneous tissue for MC simulation is shown in Fig. 1. This subcutaneous model is set from a cross-sectional view of a real human tissue with random vessel distribution. This model is established with the reference to blood casting of

Biomedical Optics EXPRESS

the human wrist, as shown in Fig. 1(a). Circular vessels with different diameters are randomly distributed in a rectangular tissue, which is similar to a plum pudding model. The entire model is 10-cm wide (x axis) and 2-cm thick (y axis), and the blood vessels are represented by circles with different diameters. A light source with 850 nm wavelength set at the coordinate position (0,0), as shown in Fig. 1(b). There are two reasons for picking 850 nm as the simulating light wavelength. First, light with 850-nm wavelength is easy to scatter by the components in the blood vessel [31]. Second, compared to the scattering and absorbing by the blood vessel, the other tissues have little influence on the light [32,33]. In the MC simulation, we set the intensity of one beam light as 1 and repeat to track the path of the photon in the tissue more than 10,000 times. During the light propagation, not only is the intensity of the light attenuated by the tissue or blood vessel absorption, but also the orientation of light propagation is changed by scattering effects of the tissue or blood vessel. In general, some light beams are reflected by the tissue, and they exit on the same side as the input light; other beams are transmitted through the tissue, and they exit at the opposite side of the input light.

Table 1. Parameters used in the MC simulation

Quantity	Symbol	Value	Unit
Constants in MC simulation			
Tissue absorption coefficient	μ_{at}	0.001	cm^{-1}
Vessel absorption coefficient	μ_{vt}	0.415	cm^{-1}
Tissue scattering coefficient	μ_{st}	10	cm^{-1}
Vessel scattering coefficient	μ_{sv}	360	cm^{-1}
Tissue anisotropy of scattering	μ_{sat}	0.2	
Vessel anisotropy of scattering	μ_{sav}	0.95	
Variates in MC simulation			
beam quantity	n	$1e^3 – 2e^4$	
Light incident angle	θ	0 – 45	degree
Light source range		0 – 60	μm
Light source size	l_s	0.1 – 1	mm
Vessel diameter	d_v	10 – 90	μm
Vessel density	ρ_v	10 – 250	mm^{-2}
Vessel range	σ_v	0 – 60	μm

In this work, we repeat the MC simulation with different parameters of vessels and light source, and then investigate their influences on the characteristics of reflected and transmitted light. The variations in simulation include the parameters that will be changed by deformation, such as incident angle, range and vessel diameter. The other parameters which are independent of the deformation remain unchangeable, such as the absorbing coefficient of the blood vessel. All the parameters are listed in Table 1 [27,34]. Before the MC simulation, we make four assumptions about the light transmission in human tissue. First, the substances in the tissue or blood vessel are homogenous, which means that light is uniformly absorbed in the tissue or vessel. Second, all lights reaching the tissue begin as ballistic lights, and the

Biomedical Optics EXPRESS

optical characteristics are unchanged during propagation in tissue. Third, the scattering of the light is anisotropic. Fourth, the interface of the tissue model will not influence the light propagation. The probability of scattering can be calculated by the scattering coefficient μ:

$$P_s = 1 - e^{-\mu d} \tag{1}$$

where d is the migrating distance. If the scattering occurs, the scattering angle is determined by $s \cdot \cos(\mu_s)$, where μ_s and s are the anisotropy of scattering and the random number from group (–1,1), respectively. In each step of the migration, light intensity is attenuated by the tissue and vessels:

$$I_{new} = I_{old} \bullet e^{-\mu_a} \tag{2}$$

where the μ_a is the absorption coefficient. Combining the scattering and absorbing factors, the position and intensity of the light can be determined after each migration. Figure 1(c, d) show the propagation of one beam. The propagating orientation is changed by the scattering owing to the tissue and vessel.

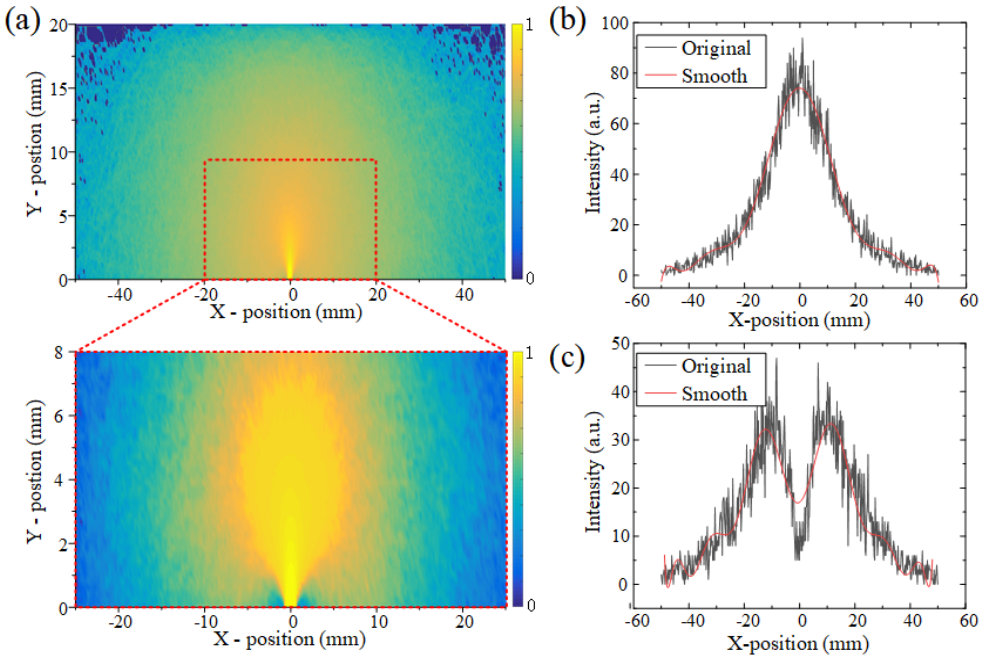

Fig. 2. (a) Cloud maps of the light intensity in human tissue. In red rectangle: the zoom-in map in the range of x(–25,25) with normalized intensity. The distribution of (b) Transmitted and (c) reflected light along the horizontal x axis.

3. Modeling methods

The simulation starts with the building of a subcutaneous model. First, we divided a rectangular box of 100 mm width and 20 mm height in a grid. This grid determines the density of the blood vessel. Then we created a circular blood vessel in each grid; the diameter of the blood vessel was no larger than the length or size of each grid. Blood vessels of different sizes can be generated by adding a random difference to the original diameter. The blood vessels and other tissues have different scattering and absorbing effects on light. So, within or without the blood vessel, different coefficients were used. Thus, we set up the 2D tissue model.

Biomedical Optics EXPRESS

Each beam of light was generated within the section of the LED. The light beams were sequence emitted into the tissue with designed incident parameters. During the propagation of light transmission in the tissue, we judged the state of the beam propagation, including the propagating angle and intensity. The step length was 1 μm in the tissue and blood vessel, which means the beam parameters were calculated after 1 μm propagating length. We obtained the sum of the light intensities on the reflection and transmission sides per 500 μm width, and then smoothed the curve of intensity distribution with the polynomial fitting method.

4. Simulation results

We traced the propagation of $1e^4$ beams and marked the light intensity at each points in the subcutaneous tissue. The cloud map of the light intensity is shown in Fig. 2(a). The initial intensity of each beam is set as one. The light intensity at each point on the cloud map depend on the sum of light intensities at that position. The distribution of light intensity is independent of the parameters of the vessels and incident light. Most initial beams propagate along the *y*- axis, then disperse slowly at different orientation. Some light beams are absorbed by the subcutaneous tissue, and others exit at the transmission or reflection side. These transmitted and reflected light beams carry information of vital signs after interacting with the tissue and blood vessel. The characteristics of these light beams will be fully investigated in this work. Changes in vessel parameters will directly influence the light distribution in the tissue. The light intensity is more separated when the vessel density is 200 mm^{-2} (Fig. 2(a)), compared with our previous work with a density of 100 mm^{-2} [35].

The accuracy of the skin-like device is sensitive to the intensity of exited light. The maximum reflected or transmitted light beams are the optimal working points for high accuracy and sensitivity. When the skin suffers external stress such as squeezing or twisting, the density and diameter of the blood vessels will change. As a result, the characteristics of the exited light beams will be influenced. Figure 2(b, c) illustrate the typical intensity distribution of the reflected and transmitted light intensity. To measure the light intensity distributed along the *x*-axis, we divide the reflected and transmitted edge into 0.2-mm intervals, and measure the light intensities at each interval to obtain the distribution of the output lights. To investigate the maximum points of the exited light intensity, we used different methods to fit the counted distribution curves, including an adaptive smooth filter, cubic spline interpolation and polynomial fitting. Finally, the polynomial fitting method is chosen for the next analysis for the smoothness. Under the condition of vertical incidence into the tissue, both the curves of reflection and transmission are axisymmetric to the light incident position. The *x*-position of the maximum transmitted intensity is the same as the light source. There are two extreme points on the reflected curves, and their intensities are approximately the same. The influence of the skin or device deformation on these two curves will be comprehensively discussed below.

In this work, we analyzed the relationship of the maximum exited light and tissue deformation, as shown in Fig. 3. We set the changeable characteristics of blood vessels to simulate the influence of tissue deformation. We repeated the simulation of light propagation with different diameters and densities of the blood vessels and summarized the characteristics of exited light intensity. The density and diameter were changed from 10 mm^{-2} to 250 mm^{-2} and 5 μm to 50 μm, respectively. The position of maximum reflected light, which represents the x-direction distance from the center of the light source to the maximum exiting light, increases with lower vessel density and smaller vessel diameter, as shown in Fig. 3(a). It is important to note that the position change along with the vessel parameters is nonlinear. For example, the position increases slowly while the density is higher than 50 mm^{-2}, while rapid growth appears when the density is lower than 50 mm^{-2}. The trend of the change is similar to an exponential function. The maximum intensity of reflected light increases for higher vessel density and larger vessel diameter. The intensity change along with vessel parameters is

Biomedical Optics EXPRESS

approximately linear, as shown in Fig. 3(b). The characteristics of maximum transmitted light are shown in Fig. 3(c, d). The position of transmitted light remains unchanged with different densities and diameters of vessel. The maximum transmitted intensity increases for lower vessel density and diameter. The change of intensity is also similar to an exponential function. In the simulation, the maximum reflected and transmitted intensities are approximately 80 mm^{-2} and 500 mm^{-2}, which appear at coordinates (8, 0) and (0, 0) respectively. The exited maximum photons are only in proportions of 0.8% and 5% of the incident lights, which implies that most of the photons are absorbed by the blood vessel and tissue. In conclusion, the quantities of blood vessel diameter and density will change the characteristics of the maximum exited light, and the relationship between the vessel and the exited light is nonlinear.

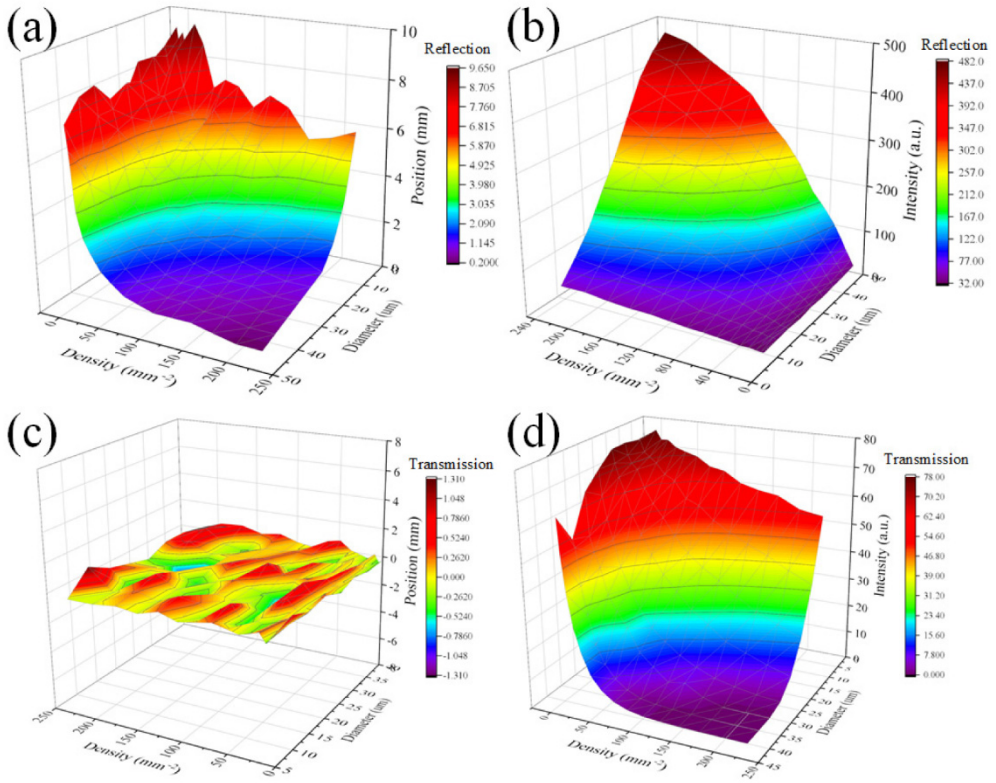

Fig. 3. 3D color maps to show the relationship between maximum exited light and blood vessel parameters. The maximum (a) position and (b) intensity at the reflected side, and the maximum (c) position and (d) intensity at the transmitted side.

Biomedical Optics EXPRESS

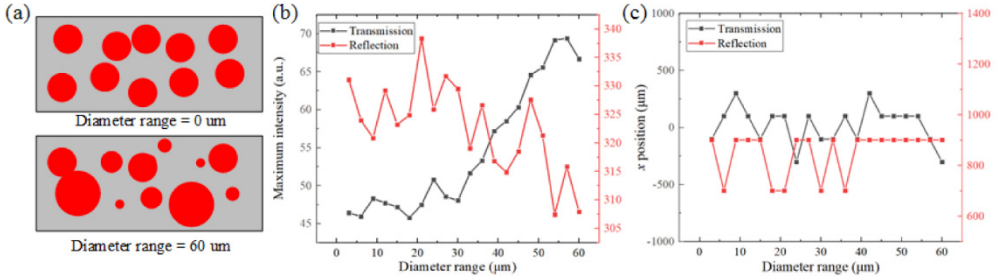

Fig. 4. The characteristics of maximum reflected and transmitted light at different diameter range. (a) Illustration of vessel distribution with different range of diameter. (b) The intensity and (c) *x*-position of the maximum exited light at different diameter range.

The deformation of blood vessels is complex in a realistic tissue under external stress. For instance, the diameters of blood vessels will be rearranged under stress. To investigate the influence of the diameter's range on exited light, we simulated the light propagation at different range of the diameter, as shown in Fig. 4. Figure 4(a) illustrates the model of a different range of vessel diameters. In this simulation, we set the mean vessel diameter as 60 μm, the vessel density as 250 mm^{-2}, and the diameter range changes from 0 μm to 60 μm. Figure 4(b, c) shows the maximum intensity and *x*- position as a function of diameter range while keeping the other parameters constant. As a result, the maximum intensity changes of transmitted and reflected light are opposite while the diameter range increases. The transmitted intensity increased from 307 to 338, and the reflected intensity decreased from 65 to 47. The influence of the diameter range is proportional to the quantity of exited intensity. The transmission intensity changes only by 8.9%, while the reflection changes by approximately 30%. Both *x*-positions are constant while the diameter range changes, which means the maximum position is independent of the diameter range, as shown in Fig. 4(c).

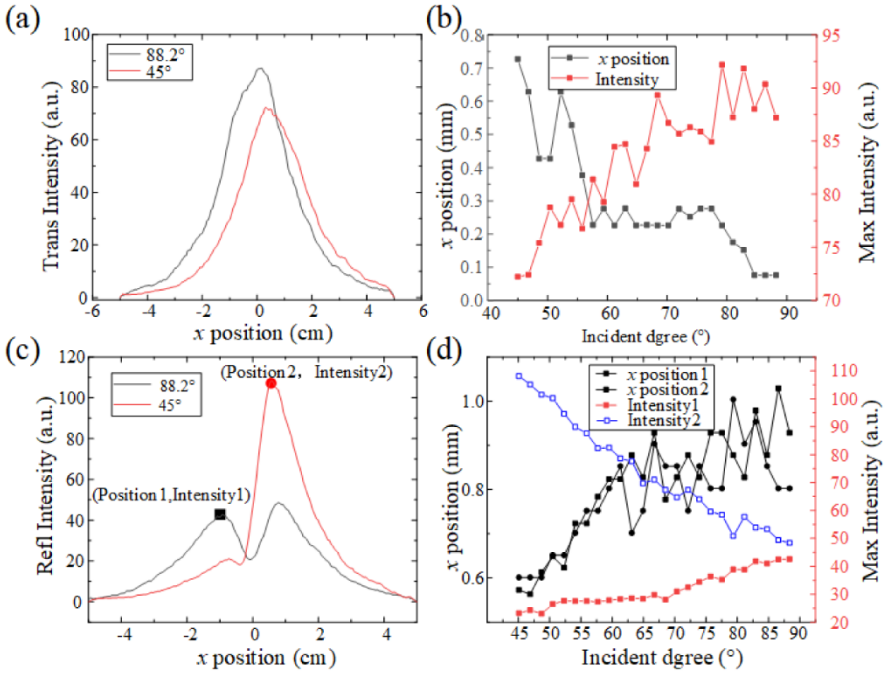

Fig. 5. The characters of transmitted (a, b) and reflected (c, d) lights as a function of incident angle.

Biomedical Optics EXPRESS

When the skin-like device deforms, the typical parameters, including incident angle, light intensity, and size, of the incident light will change. To fully investigate the influence on the accuracy of the skin-like device, we simulated the influence of device deformation on the transmitted and reflected light. The characteristics of the exited light for different incident light beams are shown in Fig. 5. The vertical and oblique incidence angles are 90° and 45°, respectively. Figure 5(a) is the distribution of the transmitted light with 88.2° and 45° incident angles. The *x*-position and maximum intensity shifts 0.7 mm and 15, respectively, while the incident angle increases from 45° to 88.2°. In general, incident angle changes have little influence on the transmitted light, as shown in Fig. 5(b). The distribution of the reflected light exists with two extremums, which appear at each side of the incident point. The reflected intensity is in nearly axisymmetric distributions of curvature with a 90° incident angle, and this axial symmetry is broken when the incident angle decreases, as shown in Fig. 5(c). Figure 5(d) illustrates the changes of the two extremums with the different incident angles. The intensities of the two extremums are equal when the incident angle reaches 90°. The two extremums change by 100% while the incident angle changes from 45° to 90°. The *x*-position of the two extremums only changes by 0.4 mm, which means that incident angles have little influence on position.

The size of the light source and intensity are also related to the characteristics of transmitted and reflected light. We simulated the *x*-position and intensity of the maximum exited light with different incident light properties, as shown in Fig. 6. The size of the light source ranged from 0.1 to 1 mm. Size of light source had little influence on intensity and position of the maximum reflected or transmitted light. The incident light intensity from $1e^3$ to $2e^4$ is proportional to the intensity of transmission and reflection. In conclusion, the characteristics of the exited light are independent of size of the light source, and the intensity is determined by incident light intensity.

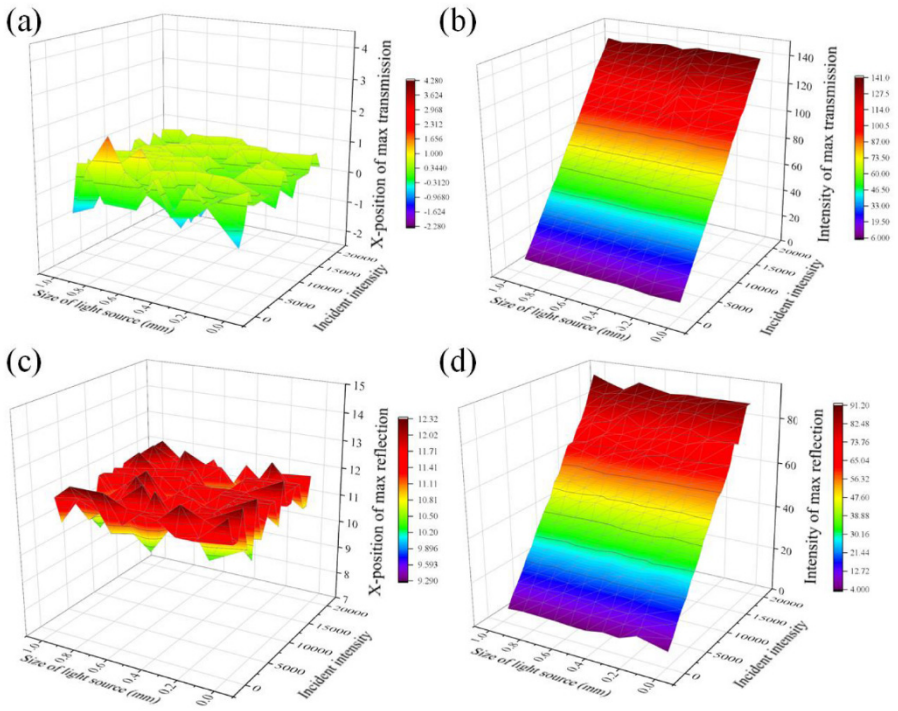

Fig. 6. Three-dimensional color map of the characteristics of maximum intensity as a function of incident light intensity and size. (a) Position and (b) intensity of the maximum transmitted light, (c) position and (d) intensity of the maximum reflection light.

Biomedical Optics EXPRESS

4. Design of the skin-like optical device

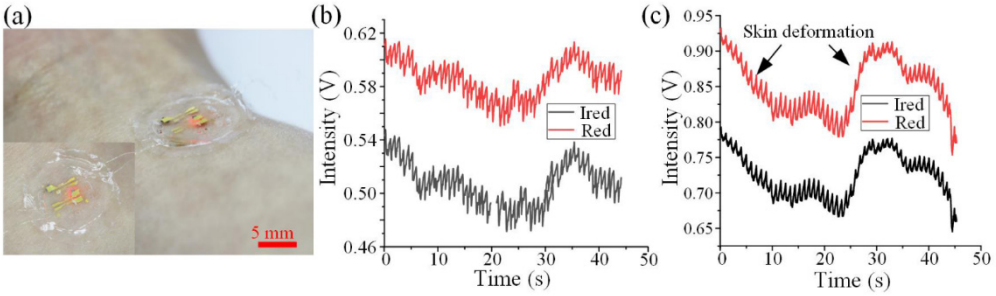

Fig. 7. (a) Skin-like optical device designed via the simulation results. Inset: zoom-in pictures of the skin-like device. (b) PPG signals of red light and infrared light detected by the skin-like optical device. (c) PPG signals detected during skin deformation.

Based on the above simulation analysis, we designed and fabricated a skin-like optical device that is capable of measuring PPG signals. Two LEDs and one photodetector were integrated on a soft substrate. The distance between the LEDs and photodetector was approximately 5 mm for optimizing the measuring accuracy near the radial artery. Figure 7(a) shows the skin-like device mounted on the skin. The device is only 500 μm thick, and it's conformal to the skin. The PPG signals were detected by the skin-like device. Figure 7(b) shows the PPG signals without filtering by any low-pass or high-pass filter. The signal processing circuits are simplified for the high signal-to-noise ratio. Also, we measured the PPG signals when the device is deformed. We stretched the device mounted on the skin and recorded the PPG signals simultaneously. The PPG signals are clear enough for the calculation of vital signs such as oxygen saturation during the deformation, as shown in Fig. 7(c).

6. Conclusion

In summary, the characteristics of the exited light scattered by the human tissue were comprehensively investigated for the design of skin-like optical devices. A 2D model with a random distribution of blood vessels was created to simulate the human tissue. Different parameters of the blood vessels were used to simulate the tissue being deformed by stress loading. Also, the structural deformation of the optical device was simulated by changing parameters such as input intensity, range, and input angle. The positions and intensity of the maximum reflected and transmitted light were analyzed by the repeated simulation of light propagation. Useful information was obtained for guiding the design of the skin-like optical device, and these simulations show some results different from traditional thought. For example, the positions of the maximum reflected and transmitted light are independent of the incident angle. Finally, we fabricated a skin-like device based on the simulation results, and successfully used it to measure PPG signals. The results open up new recognition of optical devices and provide theoretical support for skin-like optical device design.

Funding

National Basic Research Program of China (Grant No. 2015CB351904); National Natural Science Foundation of China (Grant Nos. 11625207, 11320101001, 11222220).

Disclosures

The authors declare that there are no conflicts of interest related to this article

References

1. D. Akamatsu, M. Yasuda, H. Inaba, K. Hosaka, T. Tanabe, A. Onae, and F. L. Hong, "Frequency ratio measurement of 171Yb and 87Sr optical lattice clocks," Opt. Express **22**(7), 7898–7905 (2014).

Biomedical Optics EXPRESS

2. D. W. Lamb and A. Hooper, "Laser-optical fiber Bragg grating anemometer for measuring gas flows: application to measuring the electric wind," Opt. Lett. **31**(8), 1035–1037 (2006).
3. X. Wang, L. Feng, Z. Zhou, H. Li, D. Liu, Q. Wang, L. Liu, Y. Jia, H. Jiao, and N. Liu, "Real-time free spectral range measurement based on optical single-sideband technique," Opt. Express **26**(6), 7494–7506 (2018).
4. X. Liang, M. Orescanin, K. S. Toohey, M. F. Insana, and S. A. Boppart, "Acoustomotive optical coherence elastography for measuring material mechanical properties," Opt. Lett. **34**(19), 2894–2896 (2009).
5. M. B. Aldrich, M. V. Marshall, E. M. Sevick-Muraca, G. Lanza, J. Kotyk, J. Culver, L. V. Wang, J. Uddin, B. C. Crews, L. J. Marnett, J. C. Liao, C. Contag, J. M. Crawford, K. Wang, B. Reisdorph, H. Appelman, D. K. Turgeon, C. Meyer, and T. Wang, "Seeing it through: translational validation of new medical imaging modalities," Biomed. Opt. Express **3**(4), 764–776 (2012).
6. H. Song, Y. Liu, B. Zhang, K. Tian, P. Zhu, H. Lu, and Q. Tang, "Study of in vitro RBCs membrane elasticity with AOD scanning optical tweezers," Biomed. Opt. Express **8**(1), 384–394 (2016).
7. L. Feng, J. Wang, Y. Zhi, Y. Tang, Q. Wang, H. Li, and W. Wang, "Transmissive resonator optic gyro based on silica waveguide ring resonator," Opt. Express **22**(22), 27565–27575 (2014).
8. M. Kirillin, I. Meglinski, V. Kuzmin, E. Sergeeva, and R. Myllylä, "Simulation of optical coherence tomography images by Monte Carlo modeling based on polarization vector approach," Opt. Express **18**(21), 21714–21724 (2010).
9. M. Kumar, A. Veeraraghavan, and A. Sabharwal, "DistancePPG: Robust non-contact vital signs monitoring using a camera," Biomed. Opt. Express **6**(5), 1565–1588 (2015).
10. T. Yilmaz, R. Foster, and Y. Hao, "Detecting vital signs with wearable wireless sensors," Sensors (Basel) **10**(12), 10837–10862 (2010).
11. X. Cao, X. Chen, F. Kang, Y. Lin, M. Liu, H. Hu, Y. Nie, K. Wu, J. Wang, J. Liang, and J. Tian, "Performance evaluation of endoscopic Cerenkov luminescence imaging system: in vitro and pseudotumor studies," Biomed. Opt. Express **5**(10), 3660–3670 (2014).
12. F. Litong, P. Lai-Man, X. Xuyuan, L. Yuming, and M. Ruiyi, "Motion-resistant remote imaging photoplethysmography based on the optical properties of skin," IEEE Trans. Circ. Syst. Video Tech. **25**(5), 879–891 (2015).
13. Y. Jiang, V. Reimer, T. Schossig, M. Angelmahr, and W. Schade, "Fiber optical multifunctional human-machine interface for motion capture and contact pressure monitoring," in *Advanced Photonics 2018* (BGPP, IPR, NP, NOMA, Sensors, Networks, SPPCom, SOF), OSA Technical Digest (online) (Optical Society of America, 2018), paper SeW3E.5.
14. Y. Jia, S. T. Bailey, T. S. Hwang, S. M. McClintic, S. S. Gao, M. E. Pennesi, C. J. Flaxel, A. K. Lauer, D. J. Wilson, J. Hornegger, J. G. Fujimoto, and D. Huang, "Quantitative optical coherence tomography angiography of vascular abnormalities in the living human eye," Proc. Natl. Acad. Sci. U.S.A. **112**(18), E2395–E2402 (2015).
15. V. Perekatova, P. Subochev, M. Kleshnin, and I. Turchin, "Optimal wavelengths for optoacoustic measurements of blood oxygen saturation in biological tissues," Biomed. Opt. Express **7**(10), 3979–3995 (2016).
16. Y. Khan, A. E. Ostfeld, C. M. Lochner, A. Pierre, and A. C. Arias, "Monitoring of Vital Signs with Flexible and Wearable Medical Devices," Adv. Mater. **28**(22), 4373–4395 (2016).
17. S. Y. Hong, J. H. Oh, H. Park, J. Y. Yun, S. W. Jin, L. Sun, G. Zi, and J. S. Ha, "Polyurethane foam coated with a multi-walled carbon nanotube/polyaniline nanocomposite for a skin-like stretchable array of multi-functional sensors," NPG Asia Mater. **9**, e448 (2017).
18. D. Chanda, and D. Franklin, "Imprinted Skin-Like Flexible Reflective Color Displays," in *Advanced Photonics 2016* (IPR, NOMA, Sensors, Networks, SPPCom, SOF), OSA Technical Digest (online) (Optical Society of America, 2016), paper NoM4C.4.
19. J. A. Rogers, "Wearable electronics: Nanomesh on-skin electronics," Nat. Nanotechnol. **12**(9), 839–840 (2017).
20. G. Shin, A. M. Gomez, R. Al-Hasani, Y. R. Jeong, J. Kim, Z. Xie, A. Banks, S. M. Lee, S. Y. Han, C. J. Yoo, J. L. Lee, S. H. Lee, J. Kurniawan, J. Tureb, Z. Guo, J. Yoon, S. I. Park, S. Y. Bang, Y. Nam, M. C. Walicki, V. K. Samineni, A. D. Mickle, K. Lee, S. Y. Heo, J. G. McCall, T. Pan, L. Wang, X. Feng, T. I. Kim, J. K. Kim, Y. Li, Y. Huang, R. W. Gereau 4th, J. S. Ha, M. R. Bruchas, and J. A. Rogers, "Flexible Near-Field Wireless Optoelectronics as Subdermal Implants for Broad Applications in Optogenetics," Neuron **93**(3), 509–521.e3 (2017).
21. Y. Chen, S. Lu, S. Zhang, Y. Li, Z. Qu, Y. Chen, B. Lu, X. Wang, and X. Feng, "Skin-like biosensor system via electrochemical channels for noninvasive blood glucose monitoring," Sci. Adv. **3**(12), e1701629 (2017).
22. Y. Chen, S. Lu, and X. Feng, "Skin-like nanostrucutred biosensor system for noninvasive blood glucose monitoring," *2017 IEEE International Electron Devices Meeting (IEDM)*, San Francisco, CA, (2017).
23. R. C. Webb, Y. Ma, S. Krishnan, Y. Li, S. Yoon, X. Guo, X. Feng, Y. Shi, M. Seidel, N. H. Cho, J. Kurniawan, J. Ahad, N. Sheth, J. Kim, J. G. Taylor 6th, T. Darlington, K. Chang, W. Huang, J. Ayers, A. Gruebele, R. M. Pielak, M. J. Slepian, Y. Huang, A. M. Gorbach, and J. A. Rogers, "Epidermal devices for noninvasive, precise, and continuous mapping of macrovascular and microvascular blood flow," Sci. Adv. **1**(9), e1500701 (2015).
24. Y. Chen, B. Lu, Y. Chen, and X. Feng, "Biocompatible and Ultra-Flexible Inorganic Strain Sensors Attached to Skin for Long-Term Vital Signs Monitoring," IEEE Electron Device Lett. **37**(4), 496–499 (2016).
25. Y. Chen, J. Yuan, Y. Zhang, Y. Huang, and X. Feng, "Experimental and theoretical analysis of integrated circuit (IC) chips on flexible substrates subjected to bending," J. Appl. Phys. **122**(13), 135310 (2017).
26. Y. Huang, H. Li, Y. Chen, S. Cai, Y. Zhang, B. Lu, and X. Feng, "Stretchable and flexible photonics/electronics devices and transfer printing," Scientia Sinica Physica, Mechanica & Astronomica **46**(4), 044607 (2016).

Biomedical Optics EXPRESS

27. H. Duadi, D. Fixler, and R. Popovtzer, "Dependence of light scattering profile in tissue on blood vessel diameter and distribution: a computer simulation study," J. Biomed. Opt. **18**(11), 111408 (2013).
28. F. Scholkmann, S. Kleiser, A. J. Metz, R. Zimmermann, J. Mata Pavia, U. Wolf, and M. Wolf, "A review on continuous wave functional near-infrared spectroscopy and imaging instrumentation and methodology," Neuroimage **85**(Pt 1), 6–27 (2014).
29. H. Duadi and D. Fixler, "Influence of multiple scattering and absorption on the full scattering profile and the isobaric point in tissue," J. Biomed. Opt. **20**(5), 56010 (2015).
30. http://www.dxy.cn/bbs/topic/26615112
31. G. Hong, S. Diao, J. Chang, A. L. Antaris, C. Chen, B. Zhang, S. Zhao, D. N. Atochin, P. L. Huang, K. I. Andreasson, C. J. Kuo, and H. Dai, "Through-skull fluorescence imaging of the brain in a new near-infrared window," Nat. Photonics **8**(9), 723–730 (2014).
32. R. J. Steffen, S. Sale, B. Anandamurthy, V. B. Cruz, P. M. Grady, E. G. Soltesz, and N. Moazami, "Using near-infrared spectroscopy to monitor lower extremities in patients on venoarterial extracorporeal membrane oxygenation," Ann. Thorac. Surg. **98**(5), 1853–1854 (2014).
33. J. Kim, P. Gutruf, A. M. Chiarelli, S. Y. Heo, K. Cho, Z. Xie, A. Banks, S. Han, K.-I. Jang, J. W. Lee, K.-T. Lee, X. Feng, Y. Huang, M. Fabiani, G. Gratton, U. Paik, and J. A. Rogers, "Miniaturized battery-free wireless systems for wearable pulse oximetry," Adv. Funct. Mater. **27**(1), 1604373 (2017).
34. D. J. Faber, M. C. Aalders, E. G. Mik, B. A. Hooper, M. J. van Gemert, and T. G. van Leeuwen, "Oxygen saturation-dependent absorption and scattering of blood," Phys. Rev. Lett. **93**(2), 028102 (2004).
35. H. Li, Y. Xu, X. Li, Y. Chen, Y. Jiang, C. Zhang, B. Lu, J. Wang, Y. Ma, Y. Chen, Y. Huang, M. Ding, H. Su, G. Song, Y. Luo, and X. Feng, "Epidermal Inorganic Optoelectronics for Blood Oxygen Measurement," Adv. Healthc. Mater. **6**(9), 1601013 (2017).